THE JOURNAL OF PHYSICAL CHEMISTRY B

Article

pubs.acs.org/JPCB

Excited State Proton Transfer in the Lysosome of Live Lung Cells: Normal and Cancer Cells

Rajdeep Chowdhury,[†] Abhijit Saha,[‡] Amit Kumar Mandal,[†] Batakrishna Jana,[‡] Surajit Ghosh,*[,‡] and Kankan Bhattacharyya*[,†]

[†]Department of Physical Chemistry, Indian Association for the Cultivation of Science, Jadavpur, Kolkata 700032, India

[‡]Chemistry Division, CSIR-Indian Institute of Chemical Biology, Jadavpur, Kolkata 700032, India

Supporting Information

ABSTRACT: Dynamics of excited state proton transfer (ESPT) in the lysosome region of live lung cells (normal and cancer) is studied by picosecond time-resolved confocal microscopy. For this, we used a fluorescent probe, pyranine (8-hydroxy-pyrene-1,3,6-trisulfonate, HPTS). From the colocalization of HPTS with a lysotracker dye (lysotracker yellow), we confirmed that HPTS resides in the lysosome for both of the cells. The diffusion coefficient (D_t) in the lysosome region was obtained from fluorescence correlation spectroscopy (FCS). From D_t, the viscosity of lysosome is estimated to be ~40 and ~30 cP in the cancer and normal cells, respectively. The rate constants of the elementary steps of ESPT in a normal lung cell (WI38) are compared with those in a lung cancer cell (A549). It is observed that the time constant of the initial proton transfer process in a normal cell (τ_{PT} = 40 ps) is similar to that in a cancer cell. The recombination of the geminate ion pair is slightly faster (τ_{rec} = 25 ps) in the normal cell than that (τ_{rec} = 30 ps) in a cancer cell. The time constant of the dissociation (τ_{diss}) of the geminate ion pair for the cancer cell (τ_{diss} = 80 ps) is 1.5 times faster compared to that (τ_{diss} = 120 ps) in a normal cell.

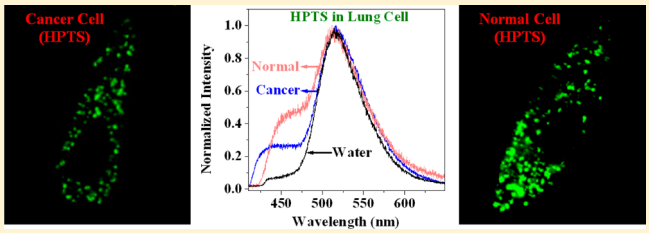

1. INTRODUCTION

Proton transfer plays a central role in many biological systems.[1−4] Proton transfer requires solvation of the ejected proton and the deprotonated species and, hence, depends on polarity of the medium. As a result of this, pK_a is extensively used to determine the polarity or dielectric constant of biological systems.[5,6] Since electron/proton transfer depends on local polarity, such mapping of pH or polarity of living systems (e.g., individual organelle in a live cell) has profound implications. The intracellular pH gradient is essential for the accumulation of many signaling agents at selected locations inside a cell. For instance, the microenvironment of the lysosome is acidic with pH ~5,[7,8] while the cytosol is slightly basic (pH ~7.4).[9] This pH gradient drives the so-called lysosomotropic agents[10] and drug molecules[11] from cytosol to the lysosome. As a result of this, in recent years, pH inside a cell[12−16] or at different interfaces has been studied by many new techniques, such as single molecule spectroscopy[15] and sum-frequency generation.[17,18]

Detailed information on the elementary steps of proton transfer may be obtained by photoinduced excited state proton transfer (ESPT).[19−36] In ESPT, one uses a probe whose ground state pK_a is large while the excited state pK_a* is low so that on excitation the probe readily loses a proton. Such a probe whose acidity may be triggered by an ultrafast laser pulse is called a photoacid. One of the most popular examples of a photoacid is pyranine (8-hydroxy-pyrene-1,3,6-trisulfonate, HPTS) with pK_a = 7.4 and pK_a* = 0.4.[21,22,25−29,31−33]

Proton transfer in the ground state has been investigated using computer simulations[37,38] and analytical theories.[39] Dynamics of ESPT in many organized and biological assemblies has been studied using techniques like picosecond time-resolved spectroscopy,[23,24] femtosecond fluorescence spectroscopy,[20,25] and femtosecond vibrational spectroscopy.[26] It is observed that mere proximity of the proton donor and acceptor in a nanocavity (e.g., cyclodextrin) is not enough. ESPT is ultrafast if the migrating proton is hydrogen bonded to the acceptor and is retarded if this hydrogen bond is interrupted.[31] Recently, there has been vigorous interest in ESPT in many biological assemblies and natural systems such as protein,[40] reverse micelle,[30] cyclodextrin,[31,32] mixed micelle,[33] and ice.[34]

Though the dynamics of ESPT has been studied in many organized assemblies, ESPT within a live cell remains vastly unexplored. Recent advancements of time-resolved confocal microscopy allow one to study dynamics inside individual locations or organelles of a live cell.[41] Very recently, we have employed this strategy to study the dynamics of ESPT inside the cytosol within a live Chinese Hamster Ovary (CHO) cell.[41]

Special Issue: Photoinduced Proton Transfer in Chemistry and Biology Symposium

Received: April 18, 2014
Revised: May 23, 2014

dx.doi.org/10.1021/jp503804y | J. Phys. Chem. B XXXX, XXX, XXX−XXX

In this work, we focus on ESPT in the organelle, lysosome inside a live cell. The dynamics of ESPT inside the lysosome region of a live cell has not been reported earlier. Lysosome is one of the most important organelles in a mammalian cell.[42,43] The lysosome contains around 50 hydrolytic enzymes which digest a wide variety of biomacromolecules (carbohydrate, protein, lipid, nucleic acid, etc.). We will show that HPTS resides in lysosome of the human lung cells (both cancer and normal cells). We have investigated a lung cancer cell (A549) and a noncancer cell, lung fibroblast cell, WI38.[44] We compare the results with our recent study on solvation dynamics inside human lung cells (both cancer and normal cells).[44] The region dependent dynamics is studied using a microscope with a spatial resolution of ~200 nm. This may eventually unravel the functions of different organelles in a live cell.

2. EXPERIMENTAL SECTION

2.1. Materials. Pyranine (8-hydroxypyrene-1,3,6-trisulfonate, HPTS, Scheme 1A, Fluka) and lysotracker yellow (Scheme 1B, invitrogen) were used without further purification.

Scheme 1. Molecular Structure of (A) 8-Hydroxypyrene-1,3,6-trisulfonate (HPTS) and (B) Lysotracker Yellow

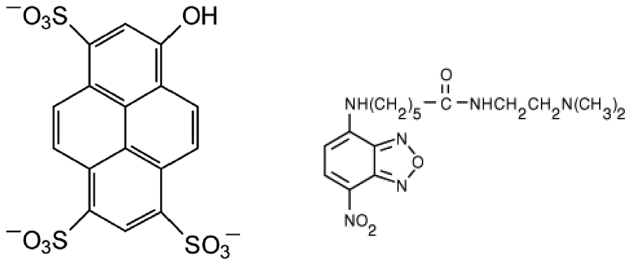

(A) (B)

2.2. Methods. *A. Cell Preparation.* Lung cancer (A549) cells and lung fibroblast (WI38) cells were grown in phenol red free DMEM (Dulbecco's Modified Eagle Medium)[44] with 10% fetal bovine serum, 1% Pen Strep Glutamine (from Gibco) in an atmosphere of 5% (v/v) CO_2 enriched air at 37 °C. Stock solutions of HPTS and lysotracker (500 nM) in media were prepared. Cancer and normal cells were seeded at a density of 5000 cells per Petri dish (BD BioCoat) for 24 h before the dye treatment. For proper staining of the cells, 200 μL of 500 nM dye solution was added to the culture dish and incubated (overnight for HPTS and 15 min for lysotracker). After incubation, the cells were washed three to four times with phosphate buffered saline (PBS) to eliminate a trace amount of dye outside the cell surface and 200 μL of fresh media was added to the Petri dish. For FCS studies, 200 μL of the 50 nM dye solutions was added to the Petri dish. Each experiment was repeated three times. All sets of experiments were executed side by side under exactly identical conditions (20 °C) so that the results can be compared without any ambiguity.

In order to prevent the photodamage of live cell by the high power of a laser, we have recorded the confocal images at a very low laser power of ~100 nW. The possibility of any autofluorescence arising from the media is eliminated by the use of phenol red free DMEM (Dulbecco's Modified Eagle Medium) media.

B. Confocal Microscope. Our confocal microscope (PicoQuant, Microtime-200) has been described in detail in our previous publication.[41]

C. Picosecond Time-Resolved Fluorescence Decays under a Microscope. In our setup, the components of fluorescence with polarization parallel ($I_{\parallel}$) and perpendicular ($I_{\perp}$) to the polarization of the exciting light were separated using a polarizing beam splitter and were monitored simultaneously using the two detectors (Micro Photon Device, MPD). Subsequently, they were combined to generate the fluorescence lifetime decays under magic angle condition as follows.[44]

$$I_{magic}(t) = I_{\parallel}(t)\cos^2(54.75^0) + I_{\perp}(t)G\sin^2(54.75^0) = (1/3)I_{\parallel}(t) + (2/3)GI_{\perp}(t) \quad (1)$$

The G value was obtained by tail matching of $I_{\parallel}$ and $I_{\perp}$ components of fluorescence intensity of HPTS in water and was found to be ~1.2. The fluorescence transients (recorded at 450 and 510 nm) were deconvoluted using the temporal response (IRF) of the detectors at 405 nm. For this purpose, we used backscattered light from a bare slide using a laser diode that emits at 405 nm. The full width at half-maxima (fwhm) of the IRF is found to be ~100 ps.

The anisotropy function, $r(t)$, was obtained under the microscope using the formula

$$r(t) = \frac{I_{\parallel}(t) - GI_{\perp}(t)}{I_{\parallel}(t) + 2GI_{\perp}(t)} \quad (2)$$

Fluorescence decay and anisotropy decay have been analyzed using DAS6 v6.3 software.[44]

D. Analysis of FCS Traces. In FCS, the autocorrelation function $G(\tau)$ of fluorescence intensity is defined as

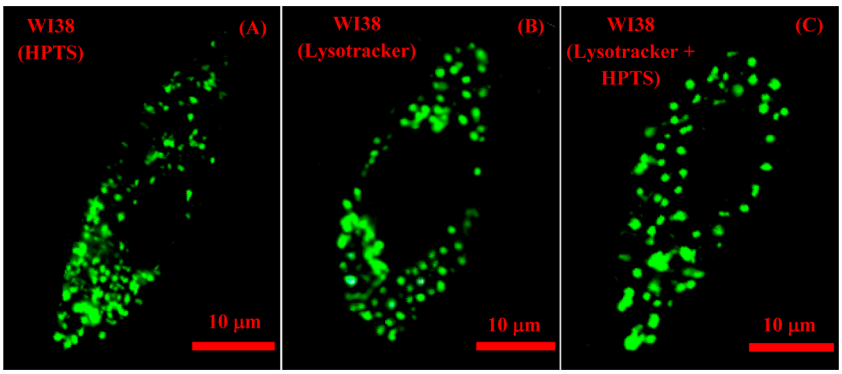

Figure 1. Confocal images of WI38 cell stained by (A) HPTS, (B) lysotracker yellow, and (C) both HPTS and lysotracker yellow.

dx.doi.org/10.1021/jp503804y | J. Phys. Chem. B XXXX, XXX, XXX−XXX

$$G(\tau) = \frac{\langle F(0)F(\tau)\rangle}{\langle F\rangle^2} \quad (3)$$

where $F(0)$ and $F(\tau)$ denote the intensity of fluorescence at time 0 and at a lag time τ, respectively.

3. RESULTS

3.1. Confocal Images: Cancer and Normal Cells. The confocal images of the cells, WI38 and A549 stained by HPTS are given in Figures 1 and 2, respectively. It is readily seen that

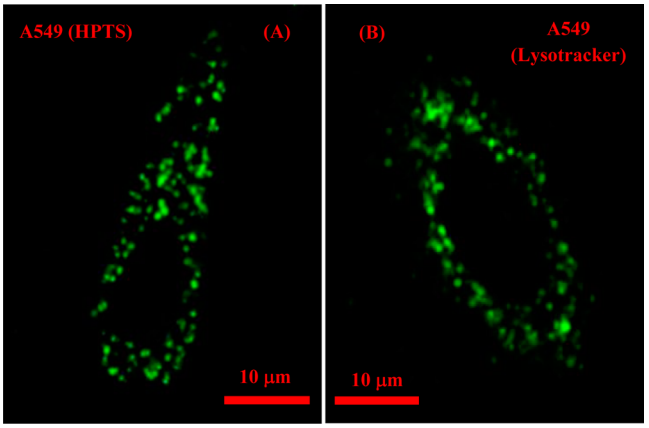

Figure 2. Confocal images of A549 cell stained by (A) HPTS and (B) lysotracker yellow.

the fluorescence probe HPTS appears as granular green blobs (with emission maximum ~510 nm). This is qualitatively different from a diffuse illumination over the entire cytoplasm obtained for HPTS in CHO cell[41] and for A549 and WI38 cells stained by coumarin 153 or nile red.[44] The granular nature in the images suggests that the dye HPTS is localized in certain specific organelles inside the A549 and WI38 cells.

The images of both of the cells stained by HPTS resemble the images of a cell whose lysosome is stained by a dye.[45] In order to prove the location of HPTS in the lysosome conclusively, we have stained the WI38 cells by a lysotracker dye (lysotracker yellow, Figure 1B,C). The images in Figure 1 clearly indicate that both HPTS and lysotracker yellow are localized in the same region of the WI38 cell. Figure 2 shows images of A549 cells stained by HPTS and lysotracker yellow dye.

The localization of the HPTS in the lysosome is further confirmed from the emission spectra recorded under the confocal microscope. Note that the emission spectra recorded under a microscope correspond to a small focused region (~200 nm). Figure 3 shows emission spectra of the WI38 cell stained by only HPTS, only lysotracker yellow, and both HPTS and lysotracker yellow, all recorded under a microscope. The emission spectrum (Figure 3C) (with both HPTS and lysotracker yellow) is a superposition of the emission spectrum of Figure 1A (only HPTS) and Figure 1B (only lysotracker yellow). Figure 3C suggests that both HPTS and lysotracker are simultaneously present in the 200 nm region. Since the lysotracker dye is known to localize in the lysosome,[45] we conclude that HPTS also localizes in the lysosome. We did not attempt to extract lysosomes using biochemical methods because our aim is to obtain information under in vivo conditions and not in isolated lysosomes.

3.2. FCS Study: Translational Diffusion in Cancer and Normal Cells. Figure 4 shows normalized autocorrelation

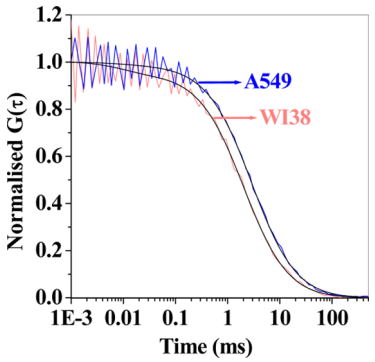

Figure 4. Normalized FCS traces of HPTS in lung cancer cell (blue) and normal lung cell (red). Corresponding fit lines are shown in solid black lines.

curves of HPTS molecules inside a single cancer (A549) and a normal (WI38) cell. From the $G(0)$ value of the FCS trace, the number of molecules in the confocal volume (N) is calculated to be ~5.

The autocorrelation traces are fitted to a 3D-diffusion model[41,46] having triplet contribution as[41]

$$G(\tau) = \frac{1 - T + \exp(-\tau/\tau_{tr})}{N(1 - T)}(1 + \tau/\tau_D)^{-1}(1 + \tau/\tau_D S^2)^{-1/2} \quad (4)$$

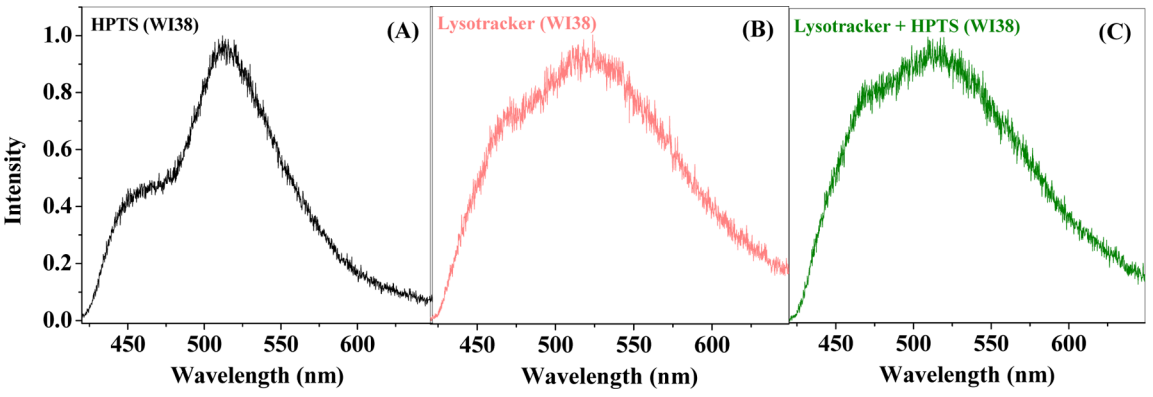

Figure 3. Emission spectra of (A) HPTS, (B) lysotracker yellow, and (C) both HPTS and lysotracker yellow inside the lysosome of WI38 cell.

dx.doi.org/10.1021/jp503804y | J. Phys. Chem. B XXXX, XXX, XXX−XXX

In the above equation, τ_D denotes the diffusion time in the confocal volume, τ_{tr} is the triplet lifetime of a dye molecule, T is the fraction of molecules in the triplet state, τ is the delay time, and N represents the average number of molecules in the confocal volume. S $(=\omega_z/\omega_{xy})$ is the structure parameter of the excitation volume, and ω_z and ω_{xy} are longitudinal and transverse radii, respectively. S is calibrated using rhodamine 6G (R6G) in water and is found to be 5.

The diffusion constant (D_t) of dye molecule was determined using the following equation

$$D_t = \frac{\omega_{xy}^2}{4\tau_D} \quad (5)$$

where ω_{xy} is the transverse radius (~320 nm) of the confocal volume (~0.9 fL). The value of ω_{xy} for our microscope was determined using R6G in water whose D_t value (426 $\mu m^2/s$)[41] is known.

Diffusion coefficient (D_t) values are calculated from the τ_D values using eqs 4 and 5. The fitting parameters are summarized in Table 1.

Table 1. FCS Data: Diffusion Time (τ_D), Triplet Fraction (T), Triplet Lifetime (τ_{tr}), Diffusion Coefficient (D_t) of HPTS, Transverse Radius (ω_{xy}), and Viscosity (η) in Lysosome

cell	τ_D[a] (ms)	D_t[a] (μm^2 s^{-1})	T	τ_{tr} (μs)	ω_{xy} (nm)	η (cP)
normal (WI38)	2.1	12	0.05	10	320	30
cancer (A549)	3	8.5	0.02	10	320	40

[a] ±10%.

In bulk water, the diffusion coefficient (D_t) of HPTS is ~350 μm^2 s^{-1}. D_t of HPTS decreases nearly 30 times to 12 μm^2 s^{-1} inside the lysosome of normal cell and by 40-fold to 8.5 μm^2 s^{-1} inside the lysosome of cancer cell. From these values of D_t, we estimated the viscosity (η) inside the lysosome of the live cell by applying the Stokes–Einstein equation. According to the Stokes–Einstein equation, the diffusion coefficient (D_t) is related to the hydrodynamic radius (r_H) as follows.[47]

$$D_t = \frac{k_B T}{6\pi\eta r_H} \quad (6)$$

where η is the viscosity of the medium. Assuming the r_H of HPTS inside the lysosome is the same as that in bulk water, the viscosity experienced by HPTS inside the lysosome of a live cell may be given by

$$\frac{\eta_{lysosome}}{\eta_{water}} = \frac{D_t^{water}}{D_t^{lysosome}} \quad (7)$$

Subscripts in η and superscripts in D_t indicate the medium in which the probe resides. Thus, the viscosity of lysosome is calculated to be ~40 and ~30 cP inside the lysosome of cancer cell and normal cell, respectively. It is evident that the viscosity of the lysosome in the lung cancer cell is slightly larger than that in the normal lung cell. Figure 5 shows the diffusion coefficient (D_t) values in different regions of the live cell.

3.3. Anisotropy Decay: Rotational Diffusion in Cancer and Normal Cells. Figure 6 shows the fluorescence anisotropy decays of HPTS recorded under a confocal microscope inside the lysosome of the normal and cancer cells. Since the intensity

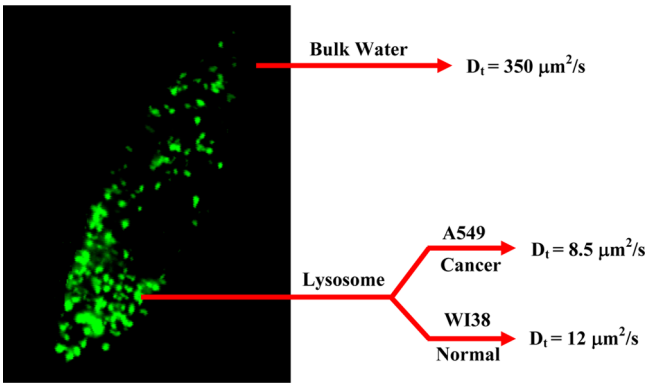

Figure 5. D_t values in different regions of a live cell and in bulk water.

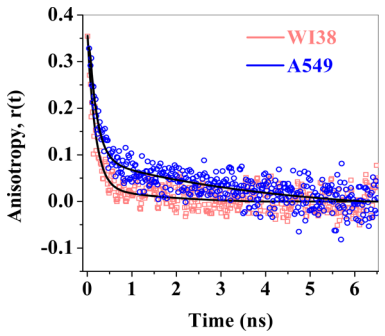

Figure 6. Anisotropy decay of HPTS inside lung cancer cell (blue) and normal lung cell (red). Corresponding fit lines are shown in solid black.

of fluorescence at ~450 nm (HA) is weak, the anisotropy decay of HPTS was monitored at ~510 nm (A^- emission). A high value of the initial anisotropy, $r(0)$, for both of the systems indicates that most of the rotational relaxation dynamics is captured in our picosecond setup.

The anisotropy decays have been fitted to biexponential as follows.

$$r(t) = r(0)[a_{1R}\exp(-t/\tau_{1R}) + a_{2R}\exp(-t/\tau_{2R})] \quad (8)$$

The parameters for anisotropy decay are summarized in Table 2. The anisotropy decay of HPTS inside the lysosome of

Table 2. Fluorescence Anisotropy Decay of HPTS (at λ_{ex} = 405 nm) in Lysosomes of Normal Cell (WI38) and Cancer Cell (A549) (λ_{em} = 510 nm)

system	$r(0)$	τ_{1R}[a] (ps) (a_{1R})	τ_{2R}[a] (ps) (a_{2R})	$\langle\tau_R\rangle$ (ps)
WI38	0.36	200 (0.85)	2000 (0.15)	470
A549	0.33	180 (0.7)	4000 (0.3)	1330

[a] ±10%

normal lung cell exhibits two time constants: τ_{1R} ~ 200 ps (0.85) and τ_{2R} ~ 2000 ps (0.15) with $\langle\tau_R\rangle$ $(=a_{1R}\tau_{1R} + a_{2R}\tau_{2R})$ ~470 ps. The rotational relaxation of HPTS in lung cancer cell is observed to be ~3 times slower with $\langle\tau_R\rangle$ ~ 1330 ps. The slower rotational relaxation inside the lysosome of lung cancer cell indicates higher viscosity compared to that in a normal cell. This is consistent with the FCS result, discussed in the previous section.

dx.doi.org/10.1021/jp503804y | J. Phys. Chem. B XXXX, XXX, XXX–XXX

3.4. Steady State Emission Spectra under a Confocal Microscope. Steady state emission spectra of HPTS in bulk water and inside the lysosome of cancer cell and normal cell (recorded using the confocal microscope) are shown in Figure 7. It is readily seen that the emission spectrum of HPTS in bulk

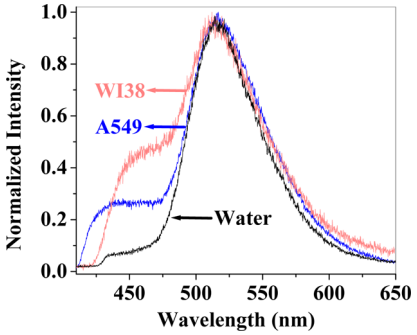

Figure 7. Normalized steady state emission spectra of HPTS in bulk water (black), inside lung cancer cell (blue), and inside normal lung cell (red).

water recorded under a microscope is almost identical to that obtained from ensemble measurements.[33] The emission spectrum of HPTS displays two peaks, one at ~450 nm (corresponding to the protonated form, HA) and another at ~510 nm (A^-). In bulk water, the emission intensity of the acid form (HA*) at 450 nm is 20 times weaker in intensity than the conjugate base form (A^{-*}) at 510 nm so that I_{510}/I_{450} ($=I_{A^-}/I_{HA}$) is 20. This is due to very rapid ESPT of HPTS in bulk water.

Inside the lung cancer cell, the intensity of emission of the HA form exhibits a marked increase so that I_{A^-}/I_{HA} is ~4; i.e., A^- (510 nm) emission is ~4 times more intense than HA (450 nm) emission. The emission intensity of the HA form is further increased inside the lysosomes of normal lung cell (WI38) to exhibit an I_{A^-}/I_{HA} ratio of ~2. This difference in the value of the I_{A^-}/I_{HA} ratio may be due to the difference in the dynamics of ESPT which will be discussed later.

In summary, we demonstrate that even in the acidic organelle lysosome (pH ~ 5) of a live cell proton can be ejected from a suitable photoacid. This is because of the fact that the excited state pK_a^* of HPTS (~0.4) is lower than the pH (~5)[7,8] of the lysosome.

3.5. Time Resolved Study under a Microscope. The steady state emission spectra qualitatively indicate that the dynamics of ESPT in the cancer cell is different compared to that in the normal cell. The rate of proton transfer inside a normal lung cell and a lung cancer cell is determined from the picosecond fluorescence transients under a confocal microscope. The picosecond transients of HA emission (λ_{em} = 450 nm) and A^- emission (λ_{em} = 510 nm) of HPTS inside the lysosome of a lung cancer cell and a normal lung cell are shown in Figure 8.

Picosecond decays of HA (at 450 nm) and A^- (at 510 nm) are fitted to a triexponential as follows.

$$I_{HA}(t) = \sum_{i=1}^{3} a_i e^{-t/\tau_i} \quad \text{and} \quad I_{A^-}(t) = \sum_{i=4}^{6} a_i e^{-t/\tau_i} \tag{9}$$

The decay parameters are summarized in Table 3. Inside the lysosome of a cancer cell, HPTS exhibits a rise time of ~200 ps. This is faster than the rise time of ~320 ps observed for a normal lung cell.

Table 3. Decay Parameters of HA and A^- Emission in the Lysosome of Different Cell Lines

cell line	species	τ_1 (a_1)[a] (ps)	τ_2 (a_2)[b] (ps)	τ_3 (a_3)[b] (ps)
W138	HA	15 (0.10)	320 (0.20)	2600 (0.70)
	A^-	15 (−0.06)	320 (−0.30)	3600 (1.36)
A549	HA	15 (0.22)	200 (0.45)	2200 (0.33)
	A^-	15 (−0.05)	200 (−0.25)	3800 (1.30)

[a]As obtained from ref 25. [b]±10%

4. DISCUSSION

In this work, we report for the first time the dynamics of excited state proton transfer within the lysosome region of a live cell.

From the FCS data, the viscosity of the lysosomal region is estimated to be ~40 cP in the lung cancer cell and ~30 cP in the normal lung cell. From the viscosity dependence of fluorescence lifetime, Deng and co-workers previously estimated the viscosity inside the lysosome of a different cancer cell (breast cancer cell) to be in the range 50−90 cP.[48] The lysosomal viscosity of the cancer cell calculated in our work is consistent with this range. This justifies the assumption that r_H of HPTS inside the lysosome of the live cell is the same as that in bulk water. However, note that our method gives a

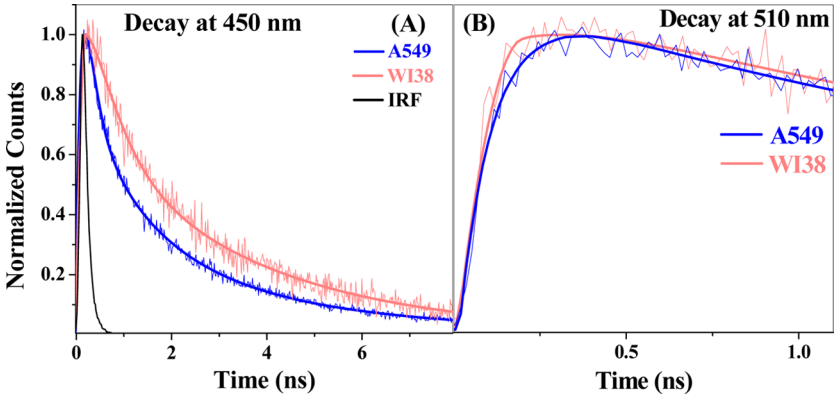

Figure 8. Picosecond transients of (A) HA emission (λ_{em} = 450 nm) and (B) A^- emission (λ_{em} = 510 nm) of HPTS in lung cell (red) and lung cancer cell (blue) at λ_{ex} = 405 nm. IRF is shown in a solid black line.

dx.doi.org/10.1021/jp503804y | J. Phys. Chem. B XXXX, XXX, XXX−XXX

precise value of lysosomal viscosity. Further, Deng and co-workers did not measure the viscosity of the lysosome in a normal cell.

Anisotropy decay also suggests that the lysosomal viscosity (friction) of the cancer cell is higher compared to the normal cell. The friction toward rotational motion (measured by anisotropy decay) in the cancer cell is 3-fold higher than that in the normal cell. However, the friction against translational motion (obtained from FCS) is only 1.3 times higher in the cancer cell. This apparent discrepancy may be reconciled as follows. Note, due to the slow diffusion coefficient in the lysosome, the HPTS molecule diffuses through a very small distance of $\sim(2D_t\tau)^{1/2}$, i.e., 0.3 nm within the excited state lifetime of the probe (~4 ns). This means the probe HPTS is essentially localized in a small area after excitation. Thus, rotational diffusion reports friction over a small distance of ~1 nm. On the other hand, translational diffusion (FCS) involves molecular motion over a longer distance of ~200 nm. Thus, FCS and anisotropy report viscosity (friction) in two different length scales. The higher viscosity in the lung cancer cell implies a more crowded environment compared to a normal lung cell.

It has been observed that, for the A549 and WI38 cells, the D_t value of HPTS inside the lysosome (~10 ± 2 $\mu m^2/s$) is close to the D_t of coumarin 153 inside the lipid droplet (~12 ± 3 $\mu m^2/s$) measured in our previous work.[44] Thus, the microenvironment in lysosome of both normal and cancer cells may be assumed to be similar to the lipid droplets (low polarity, high viscosity, and slow solvation dynamics).

The ESPT process in a photoacid (HA) involves three steps: initial proton transfer (k_{PT}), recombination (k_{rec}), and dissociation (k_{diss}) of the geminate ion pair (Scheme 2).[21,31,35,36]

Scheme 2. Kinetic Scheme Depicting the Proton Transfer Process in Pyranine (HPTS)

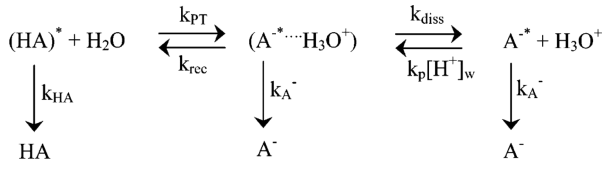

Many groups have explained geminate recombination in terms of a model involving diffusion with appropriate boundary conditions.[36,49,50] For spherically symmetric diffusion at long times, the fluorescence exhibits a power law decay ($t^{-3/2}$).[36,49,50] Fayer and co-workers reported a $t^{-0.8}$ decay for HPTS in AOT reverse micelles and Nafion film.[50] We also searched for a power law decay in the case of the two live cells: A549 and WI38. As shown in Figure 9, there is no power law decay inside the live cells. One of the possible reasons for non-power-law behavior could be the highly heterogeneous nature of the lysosome.

In order to estimate the rate constants of proton transfer, we followed a simple kinetic scheme (Scheme 2) used earlier by several groups.[21,35,36] The time evolution of the different species in Scheme 2 is described by the following coupled differential equations:[21,31]

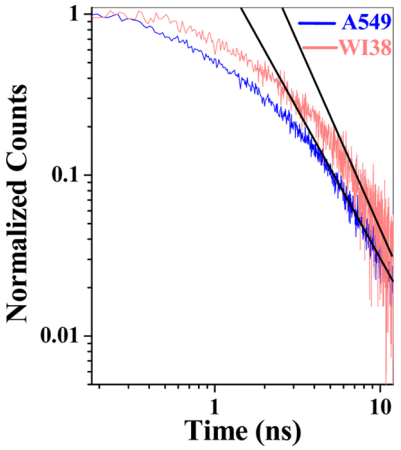

Figure 9. Decay of HA emission (450 nm) inside A549 (blue) and WI38 (red) in log–log scale.

$$\frac{d}{dt}\begin{bmatrix}HA\\A^-\cdots H^+\\A^-\end{bmatrix}=\begin{bmatrix}-X & k_{rec} & 0\\k_{PT} & -Y & 0\\0 & k_{diss} & -Z\end{bmatrix}\times\begin{bmatrix}HA\\A^-\cdots H^+\\A^-\end{bmatrix} \quad (10)$$

where

$$X = k_{PT} + k_{HA} \approx k_{PT}$$

$$Y = k_{rec} + k_{diss} + k_{A^-}$$

$$Z = k_{A^-}$$

Individual rate constants (k_{PT}, k_{rec}, and k_{diss}) were calculated using the explicit expressions (Supporting Information) involving the amplitude and decay constants of the emission transients of HA and A^-.[21,31]

The two long components (τ_2 and τ_3) and their amplitudes (a_2 and a_3) are obtained from the microscope. The ultrafast component is faster than the IRF (fwhm ~100 ps) of our time-resolved confocal microscope. The ultrafast component can be determined using the femtosecond up-conversion technique. Because of adhesion of the cells to the glass surface, they were damaged during the femtosecond up-conversion experiment even when we used a rotating cell. Therefore, for the cancer and normal cells, we assumed an ultrafast component of decay of HA is the same as that obtained for niosome, which is a good model of a cell.[25] For niosome, using femtosecond up-conversion, we have found τ_1 = 15 ps.[25] We assumed the same value of τ_1 for a live cell. We further assumed that the ratio of a_1 and a_2 amplitudes in the live cell is the same as that in the niosome. Thus, we divided a_2 (obtained in our setup of IRF ~ 100 ps) into two components in the same ratio as that in niosome.

The time constants of initial proton transfer inside the lysosome of both cells are similar (40 ps) and are about 8-fold slower than that in bulk water (5 ps) (Table 4). As shown in this work, the probe HPTS resides in the lysosomes of the lung (cancer and normal) cell. FCS results indicate that the microenvironment of the lysosome is similar to the lipid droplets. A lipid droplet is characterized by low polarity ($\varepsilon \sim 6$)[44,51] and very slow solvation (~2000–3500 ps).[44,51] This is ~2000–3500 times slower than solvation dynamics in bulk water (~1 ps[52−54]). First, the slower proton transfer in the lysosome may be attributed to a less polar environment with slower solvation compare to bulk water. Second, the excited

dx.doi.org/10.1021/jp503804y | J. Phys. Chem. B XXXX, XXX, XXX–XXX

Table 4. Time Constants of Initial Proton Transfer (τ_{PT}), Recombination (τ_{rec}) of Geminate Ion Pair and Dissociation of Ion Pair (τ_{diss}) in Bulk Water and in Different Cell Lines

system	τ_{PT}[a] (ps)	τ_{rec}[a] (ps)	τ_{diss}[a] (ps)
bulk water[b]	5	7	50
lung cell	40	25	120
lung cancer cell	40	30	80

[a] ±10%. [b] From ref 41.

state proton transfer (ESPT) requires the presence of a large number of free water molecules (as proton acceptor and for solvation) near the photoacid. It has been proposed that a proton requires at least 10 water molecules to stabilize itself and the deprotonated species (A^-) also require ~20 water molecules.[55,56] Inside the lysosome, the number of free water molecules is vastly reduced because of binding of water molecules with the biomolecules[52−54] and due to protonation of the water molecules in the acidic medium (pH ~ 5). The role of free water molecules for proton transfer has been investigated earlier by the salt effect on ESPT.[25,55]

The recombination time (τ_{rec}) in the normal cell (τ_{rec} ~ 25 ps) is slightly faster compared to that (τ_{rec} ~ 30 ps) in the cancer cell. The faster recombination time in the normal cell may be due to the less crowded and more polar environment. The time constants of recombination inside both the cancer and normal cells are slower than that (τ_{rec} = 7 ps) in bulk water (Table 4).

The time constants of dissociation in lysosome of the normal and cancer cells are ~2 times longer compared to bulk water (τ_{diss} ~ 50 ps). The slower time constant of dissociation (τ_{diss}) of the geminate ion pair inside the cells compared to bulk water may be attributed to the 30−40 times higher viscosity in the lysosome. The dissociation of the geminate ion pair in the lung cancer cell (τ_{diss} ~ 80 ps) is 1.5-fold faster than that in the normal lung cell (τ_{diss} ~ 120 ps) (Table 4). The 1.5-fold faster dissociation in a cancer cell is mainly responsible for the 2-fold higher I_{A^-}/I_{HA} ratio (Figure 7).

5. CONCLUSION

This work demonstrates that it is possible to monitor organelle specific proton transfer dynamics inside a live cell using time-resolved confocal microscopy. Using FCS, we first show that the lysosome region is characterized by very high viscosity similar to the lipid droplets. This indicates a crowded and hydrophobic environment. The variation of time constants of ESPT from that of bulk water indicates differences in polarity and solvation dynamics within lysosome. The lysosome of a cancer cell may be different in terms of polarity, solvation dynamics, and viscosity from the normal cell. As a result, the dynamics of ESPT in a cancer cell is different compared to its normal analogue. Such detailed knowledge of chemical dynamics (e.g., proton transfer) may eventually elucidate cellular processes in microscopic detail.

■ ASSOCIATED CONTENT

Supporting Information

Expressions of rate constants for elementary steps of excited state proton transfer. This material is available free of charge via the Internet at http://pubs.acs.org.

■ AUTHOR INFORMATION

Corresponding Authors

*E-mail: sghosh@iicb.res.in.

*E-mail: pckb@iacs.res.in. Fax: (91)-33-2473-2805.

Notes

The authors declare no competing financial interest.

■ ACKNOWLEDGMENTS

Thanks are due to Department of Science and Technology, India (K.B.), J. C. Bose Fellowship (K.B.), Ramanujan Fellowship (S.G.), and Council of Scientific and Industrial Research, CSIR (S.G.). R.C., A.S., A.K.M., and B.J. thank CSIR for awarding fellowships. We also thank National Centre for Cell Science (NCCS), Pune, for providing the A549 cell line and Professor Sanghamitra Raha (SINP) for kindly donating the WI38 cell line.

■ REFERENCES

(1) Il'ichev, Y. V.; Demyashkevich, A. B.; Kuzmin, M. G. Protolytic photodissociation of hydroxyaromatic compounds in micelles and lipid bilayer membranes of vesicles. *J. Phys. Chem.* **1991**, *95*, 3438−3444.

(2) Presiado, I.; Erez, Y.; Huppert, D. Excited-State Intermolecular Proton Transfer of Firefly Luciferin III. Proton Transfer to a Mild Base. *J. Phys. Chem. A* **2010**, *114*, 13337−13346.

(3) Tolbert, L. M.; Solntsev, K. M. Excited-State Proton Transfer: From Constrained Systems to "Super" Photoacids to Superfast Proton Transfer. *Acc. Chem. Res.* **2002**, *35*, 19−27.

(4) Baranov, M. S.; Lukyanov, K. A.; Borissova, A. O.; Shamir, J.; Kosenkov, D.; Slipchenko, L. V.; Tolbert, L. M.; Yampolsky, I. V.; Solntsev, K. M. Conformationally Locked Chromophores as Models of Excited-State Proton Transfer in Fluorescent Proteins. *J. Am. Chem. Soc.* **2012**, *134*, 6025−6032.

(5) Schutz, C. N.; Warshel, A. What are the dielectric "constants" of proteins and how to validate electrostatic models? *Proteins* **2001**, *44*, 400−417.

(6) Warshel, A.; Sharma, P. K.; Kato, M.; Parson, W. W. Modeling electrostatic effects in proteins. *Biochim. Biophys. Acta* **2006**, *1764*, 1647−1676.

(7) Feng, Y.; Forgac, M. A novel mechanism for regulation of vacuolar acidification. *J. Biol. Chem.* **1992**, *267*, 19769−19772.

(8) Geisow, M. Lysosome proton pump identified. *Nature* **1982**, *298*, 515−516.

(9) Bright, G. R.; Fisher, G. W.; Rogowska, J.; Taylor, D. L. Fluorescence ratio imaging microscopy: temporal and spatial measurements of cytoplasmic pH. *J. Cell Biol.* **1987**, *104*, 1019−1033.

(10) Goldman, S. D. B.; Funk, R. S.; Rajewski, R. A.; Krise, J. P. Mechanisms of amine accumulation in, and egress from, lysosomes. *Bioanalysis* **2009**, *1*, 1445−1459.

(11) Duvvuri, M.; Konkar, S.; Hong, K. H.; Blagg, B. S. J.; Krise, J. P. A New Approach for Enhancing Differential Selectivity of Drugs to Cancer Cells. *ACS Chem. Biol.* **2016**, *1*, 309−315.

(12) Overly, C. C.; Lee, K. D.; Berthiaume, E.; Hollenbeck, P. J. Quantitative measurement of intraorganelle pH in the endosomal-lysosomal pathway in neurons by using ratiometric imaging with pyranine. *Proc. Natl. Acad. Sci. U.S.A.* **1995**, *92*, 3156−3160.

(13) Han, J.; Burgess, K. Fluorescent Indicators for Intracellular pH. *Chem. Rev.* **2010**, *110*, 2709−2728.

(14) Kotlyar, A. B.; Borovok, N.; Kiryati, S.; Nachliel, E.; Gutman, M. The dynamics of proton transfer at the C side of the mitochondrial membrane: Picosecond and microsecond measurements. *Biochemistry* **1994**, *33*, 873−879.

(15) Battisti, A.; Digman, M. A.; Gratton, E.; Storti, B.; Beltrama, F.; Bizzarriz, R. Intracellular pH measurements made simple by fluorescent protein probes and the phasor approach to fluorescence lifetime imaging. *Chem. Commun.* **2012**, *48*, 5127−5127.

(16) Chen, S.; Hong, Y.; Liu, Y.; Liu, J.; Leung, C. W. T.; Li, M.; Kwok, R. T. K.; Zhao, E.; Lam, J. W. Y.; Yu, Y.; Tang, B. Z. Full-Range

Intracellular pH Sensing by an Aggregation-Induced Emission-Active Two-Channel Ratiometric Fluorogen. *J. Am. Chem. Soc.* **2013**, *135*, 4926−4929.
(17) Yamaguchi, S.; Bhattacharyya, K.; Tahara, T. Acid−Base Equilibrium at an Aqueous Interface: pH Spectrometry by Heterodyne-Detected Electronic Sum Frequency Generation. *J. Phys. Chem. C* **2011**, *115*, 4168−4173.
(18) Yamaguchi, S.; Kundu, A.; Sen, P.; Tahara, T. Quantitative estimate of the water surface pH using heterodyne-detected electronic sum frequency generation. *J. Chem. Phys.* **2012**, *137*, 151101-1−151101-4.
(19) Tran-Thi, T. H.; Gustavsson, T.; Prayer, C.; Pommeret, S.; Hynes, J. T. Primary ultrafast events preceding the photoinduced proton transfer from pyranine to water. *Chem. Phys. Lett.* **2000**, *329*, 421−430.
(20) Karton-Lifshin, N.; Presiado, I.; Erez, Y.; Gepshtein, R.; Shabat, D.; Huppert, D. Ultrafast Excited-State Intermolecular Proton Transfer of Cyanine Fluorochrome Dyes. *J. Phys. Chem. A* **2012**, *116*, 85−92.
(21) Spry, D. B.; Goun, A.; Fayer, M. D. Deprotonation Dynamics and Stokes Shift of Pyranine (HPTS). *J. Phys. Chem. A* **2007**, *111*, 230−237.
(22) Spry, D. B.; Goun, A.; Glusac, K.; Moilanen, D. E.; Fayer, M. D. Proton Transport and the Water Environment in Nafion Fuel Cell Membranes and AOT Reverse Micelles. *J. Am. Chem. Soc.* **2007**, *129*, 8122−8130.
(23) Iyer, E. S. S.; Datta, A. (2,2′-Bipyridyl)-3-3′-diol in Nafion: Stabilization of Unusual Ground and Excited States. *J. Phys. Chem. B* **2012**, *116*, 5302−5307.
(24) Iyer, E. S. S.; Datta, A. Importance of Electrostatic Interactions in the Mobility of Cations in Nafion. *J. Phys. Chem. B* **2011**, *115*, 8707−8712.
(25) Mondal, T.; Ghosh, S.; Das, A. K.; Mandal, A. K.; Bhattacharyya, K. Salt Effect on the Ultrafast Proton Transfer in Niosome. *J. Phys. Chem. B* **2012**, *116*, 8105−8112.
(26) Cox, M. J.; Siwick, B. J.; Bakker, H. J. Influence of ions on aqueous acid-base reactions. *ChemPhysChem* **2009**, *10*, 236−244.
(27) Cox, M. J.; Timmer, R. L. A.; Bakker, H. J.; Park, S.; Agmon, N. Distance-Dependent Proton Transfer along Water Wires Connecting Acid−Base Pairs. *J. Phys. Chem. A* **2009**, *113*, 6599−6606.
(28) Mohammed, O. F.; Pines, D.; Dreyer, J.; Pines, E.; Nibbering, E. T. J. Sequential Proton Transfer Through Water Bridges in Acid-Base Reactions. *Science* **2005**, *310*, 83−86.
(29) Cox, M. J.; Bakker, H. J. Parallel proton transfer pathways in aqueous acid-base reactions. *J. Chem. Phys.* **2008**, *128*, 174501-1−174501-10.
(30) Cohen, B.; Huppert, D.; Solntsev, K. M.; Tsfadia, Y.; Nachliel, E.; Gutman, M. Excited State Proton Transfer in Reverse Micelles. *J. Am. Chem. Soc.* **2002**, *124*, 7539−7547.
(31) Mondal, S. K.; Sahu, K.; Ghosh, S.; Sen, P.; Bhattacharyya, K. Excited-State Proton Transfer from Pyranine to Acetate in γ-Cyclodextrin and Hydroxypropyl γ-Cyclodextrin. *J. Phys. Chem. A* **2006**, *110*, 13646−13652.
(32) Gepshtein, R.; Leiderman, P.; Huppert, D.; Project, E.; Nachliel, E.; Gutman, M. Proton Antenna Effect of the γ-Cyclodextrin Outer Surface, Measured by Excited State Proton Transfer. *J. Phys. Chem. B* **2006**, *110*, 26354−26364.
(33) Mondal, T.; Das, A. K.; Sasmal, D. K.; Bhattacharyya, K. Excited State Proton Transfer in Ionic Liquid Mixed Micelles. *J. Phys. Chem. B* **2010**, *114*, 13136−13142.
(34) Leiderman, P.; Uritski, A.; Huppert, D. Temperature Dependence of Excited State Proton Transfer in Ice. *J. Phys. Chem. A* **2007**, *111*, 4998−5007.
(35) Eigen, M. Proton Transfer, Acid-Base Catalysis, and Enzymatic Hydrolysis. *Angew. Chem.* **1964**, *3*, 1−72.
(36) Agmon, N.; Pines, E.; Huppert, D. Geminate recombination in proton transfer reactions. II. Comparison of diffusional and kinetic schemes. *J. Chem. Phys.* **1988**, *88*, 5631−5638.
(37) Wang, S.; Bianco, R.; Hynes, J. T. Dissociation of nitric acid at an aqueous surface: Large amplitude motions in the contact ion pair to solvent-separated ion pair conversion. *Phys. Chem. Chem. Phys.* **2010**, *12*, 8241−8249.
(38) Ka, B. J.; Thompson, W. H. Sampling the Proton Transfer Reaction Coordinate in Mixed Quantum-Classical Molecular Dynamics Simulations. *J. Phys. Chem. A* **2012**, *116*, 832−838.
(39) Thompson, W. H. Solvation Dynamics and Proton Transfer in Nanoconfined Liquids. *Annu. Rev. Phys. Chem.* **2011**, *62*, 599−619.
(40) Cohen, B.; Álvarez, C. M.; Carmona, N. A.; Organero, J. A.; Douhal, A. Proton-Transfer Reaction Dynamics within the Human Serum Albumin Protein. *J. Phys. Chem. B* **2011**, *115*, 7637−7647.
(41) Sen Mojumdar, S.; Chowdhury, R.; Mandal, A. K.; Bhattacharyya, K. In what time scale proton transfer takes place in a live CHO cell? *J. Chem. Phys.* **2013**, *138*, 215102-1−215102-9.
(42) Aronson, N. N., Jr.; de Duve, C. Digestive activity of lysosomes. II. The digestion of macromolecular carbohydrates by extracts of rat liver lysosomes. *J. Biol. Chem.* **1968**, *243*, 4564−4573.
(43) de Duve, C.; Wattiaux, R. Functions of lysosomes. *Annu. Rev. Physiol.* **1966**, *28*, 435−492.
(44) Chowdhury, R.; Jana, B.; Saha, A.; Ghosh, S.; Bhattacharyya, K. Confocal microscopy of cytoplasmic lipid droplets in a live cancer cell: number, polarity, diffusion and solvation dynamics. *Med. Chem. Commun.* **2014**, *5*, 536−539.
(45) Abdul-Hay, S. O.; Sahara, T.; McBride, M.; Kang, D.; Leissring, M. A. Identification of BACE2 as an avid ß-amyloid-degrading protease. *Mol. Neurodegener.* **2012**, *7*, 46-1−46-12.
(46) Agmon, N. The residence probability: single molecule fluorescence correlation spectroscopy and reversible geminate recombination. *Phys. Chem. Chem. Phys.* **2011**, *13*, 16548−16557.
(47) Lakowicz, J. R. *Principles of Fluorescence Spectroscopy*, 3rd ed.; Springer: New York, 2006; Chapters 6, 7, 10, and 24.
(48) Wang, L.; Xiao, Y.; Tian, W.; Deng, L. Activatable Rotor for Quantifying Lysosomal Viscosity in Living Cells. *J. Am. Chem. Soc.* **2013**, *135*, 2903−2906.
(49) Pines, E.; Huppert, D.; Agmon, N. Geminate recombination in excited-state proton-transfer reactions: Numerical solution of the Debye−Smoluchowski equation with back reaction and comparison with experimental results. *J. Chem. Phys.* **1988**, *88*, 5620−5630.
(50) Moilanen, D. E.; Spry, D. B.; Fayer, M. D. Water Dynamics and Proton Transfer in Nafion Fuel Cell Membranes. *Langmuir* **2008**, *24*, 3690−3698.
(51) Ghosh, S.; Chattoraj, S.; Mondal, T.; Bhattacharyya, K. Dynamics in Cytoplasm, Nucleus, and Lipid Droplet of a Live CHO Cell: Time-Resolved Confocal Microscopy. *Langmuir* **2013**, *29*, 7975−7982.
(52) Zhong, D.; Pal, S. K.; Zewail, A. H. Biological water: A critique. *Chem. Phys. Lett.* **2011**, *503*, 1−11.
(53) Bagchi, B.; Jana, B. Solvation dynamics in dipolar liquids. *Chem. Soc. Rev.* **2010**, *39*, 1936−1954.
(54) Bhattacharyya, K. Nature of biological water: a femtosecond study. *Chem. Commun.* **2008**, 2848−2857.
(55) Leiderman, P.; Gepshtein, R.; Uritski, A.; Genosar, L.; Huppert, D. Effect of Electrolytes on the Excited-State Proton Transfer and Geminate Recombination. *J. Phys. Chem. A* **2006**, *110*, 5573−5584.
(56) Huppert, D.; Kolodney, E.; Gutman, M.; Nachliel, E. Effect of water activity on the rate of proton dissociation. *J. Am. Chem. Soc.* **1982**, *104*, 6949−6953.